AD-A250 414

‖‖‖‖‖‖‖‖‖‖‖‖‖‖

Office of Naval Research

Report for

30 November 1991 to April 15th 1992

for

Grant Number N00014-89-J-1158
R&T No. 4143117 - 01

Studies of Quantitative Methods for Imaging from Scattered Fields

Principal Investigator: M. A. Fiddy
Dept. of Electrical Engineering,
University of Massachusetts Lowell,
Lowell, MA 01854

Circulation:
Dr. A. K. Jordan (3 copies)
[Administrative Grants Officer, ONR (1 copy)   *not required under FDP]*
[Director, NRL (6 copies)   *not required under FDP]*
[Defence Technical Information Center (12 copies)   *not required under FDP]*

92-11906

‖‖‖‖‖‖‖‖‖‖‖‖‖

92   4 30 034

Summary of overall progress

The analysis of the advantages and disadvantages of the homomorphic filtering technique applied to solve the exact inverse scattering problem has continued. There have been problems with strongly scattering objects due to phase unwrapping. Work has continued to more carefully compare the reconstruction of $\nabla\Psi$ from the backpropagation of simulated data with that predicted for the direct problem, from the same data.

We note that phase unwrapping is avoided with the differential cepstrum; we believe that there might be an interesting connection between this and a novel differential formalism for the Rytov approximation.

This report focuses mainly on new developments in modelling scattering from nonlinear media. In anticipation of the next phase of this project, namely to consider the inverse scattering problem for nonlinear medium, we have been studying the writing of structures into nonlinear media, specifically photorefractive crystals. A paper on this has been rewritten following submission to JOSA-B and has now been submitted to Opt. Comp. & Sig. Proc. Both experimental and theoretical work continues toward writing structures with intense beams and reading with weak beams, the partial erasure on reading being a problem without fixing. Methods for fixing are being independently developed within the group.

1

Activities

During the last four-month period

Next July, M.A. Fiddy is chair, and F.C. Lin co-chair of the Conference on Inverse Problems in Scattering and Imaging, at SPIE's 1992 International Symposium on optical Applied Science and Engineering, in San Diego. There are 50 papers from all over he world being presented.

Papers and conference presentations

Lin, F.C. and M.A. Fiddy, "On the issue of the Born-Rytov controversy: I Comparing analytical and approximate expressions for the one-dimensional case", accepted J.O.S.A. A.

Lin, F.C. and M.A. Fidd "Optimization of the self-pumped phase conjugation in $BaTiO_3$ for optical image storage and readout", submitted to Opt. Comp. and Sig. Proc.

There are also 2 papers on inverse problems to be presented at the San Diego meeting in July.

Lin, F.C., R. McGahan, A. Alavi and M.A. Fiddy, "Quantitative image recovery and restoration from scattered field data at 10GHz," to be presented in the Conference on Inverse Problems in Scattering and Imaging, at SPIE's 1992 International Symposium on optical Applied Science and Engineering, in San Diego.

McGahan, R., F.C. Lin and M.A. Fiddy, "Cepstral filtering for recovery of object from scattered field data," to be presented in the Conference on Inverse Problems in Scattering and Imaging, at SPIE's 1992 International Symposium on optical Applied Science and Engineering, in San Diego.

Progress since last report

1.   Propagation of Light in One-dimensional Half-space Nonlinear Media

Because of their large nonlinearities observable with the usage of lower-power cw lasers, artificial Kerr media such as aqueous suspension of submicrometer dielectric spheres may be found useful as nonreciprocal media for switching, image amplification or as storage media for holographic imaging [1]. We are interested in their use as controllable scattering media for design and synthesis of optical components, in which strong scattering phenomena play a role.

Consider a laser beam incident from free-space (region 0 for $z < 0$) into the one-dimensional (1-D) half-space nonlinear medium (region 1 for $z \geq 0$) [Figure 1]. Suppose that the incident laser beam is a time-harmonic plane wave $e^{i(k_0 z - \omega t)}$ with radial frequency ω and $k_0 = \omega\sqrt{\mu_0 \varepsilon_0}$ where μ_0 and ε_0 are the free-space permeability and permittivity, respectively. Also assume that the nonlinear medium can be characterized by the free-space permeability μ_0 and a permittivity $\varepsilon_1(z) = \varepsilon_1[n_0(z) + \Delta n(z)]^2$. The spatial distribution of inhomogeneities in the medium modulates locally the linear refractive index $n_0(z)$ [1] while the effects of self-actions of light in the medium gives rise to the nonlinear term $\Delta n(z)$ [2]. For example, in artificial Kerr media such as liquid suspensions of submicrometer dielectric particles, the electrostrictive effect yields the intensity-dependent contribution to the nonlinear term, i.e.,
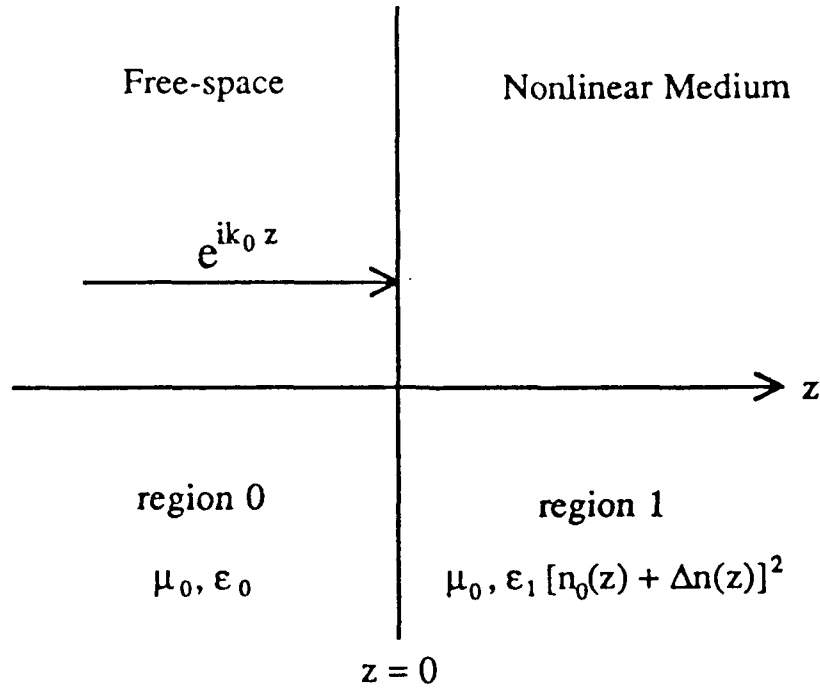
$$\Delta n(z) = \frac{n_2}{2n_1} |\Psi_1(z)|^2 \tag{1}$$

3

Free-space | Nonlinear Medium

$e^{ik_0 z}$

z

region 0 | region 1

μ_0, ε_0 | $\mu_0, \varepsilon_1 [n_0(z) + \Delta n(z)]^2$

$z = 0$

Figure 1.

where $n_1 = \sqrt{\varepsilon_1/\varepsilon_0}$ and n_2 and $\Psi_1(z)$ are the nonlinear (Kerr) constant and the total field in region 1 (the nonlinear medium), respectively. For liquid suspension of submicrometer polystyrene latex spheres with 0.234 μm in diameter, the typical value of n_2 is about 10^{-9} cm²/W [3]. Therefore, for the moderate laser intensity from 1 to 100 W/cm², $\Delta n(z)$ can be taken as a small perturbation to $n_0(z)$.

In the 1-D scattering theory, the total fields, $\Psi_0(z)$ and $\Psi_1(z)$, in region 0 and 1 satisfy the scalar wave equations

$$\frac{d^2\Psi_0(z)}{dz^2} + k_0^2 \Psi_0(z) = 0; \qquad\qquad z < 0 \qquad (2)$$

and

4

$$\frac{d^2\Psi_1(z)}{dz^2} + k_1^2 \Psi_1(z) = -k_1^2 \left\{ \left[n_0(z) + \frac{n_2}{2n_1} |\Psi_1(z)|^2 \right]^2 - 1 \right\} \Psi_1(z); \qquad z \geq 0 \qquad (3)$$

where $k_1 = \omega \sqrt{\mu_0 \varepsilon_1}$. For brevity, the time-harmonic factor $e^{-i\omega t}$ is omitted from the total fields. The term on the right-hand side of Eq. (3) is the so-called secondary source.

1.1. The Born Method for the 1-D Half-space Nonlinear Case with $n_0(z) = 1$ and $\varepsilon_1 = \varepsilon_0$ ($n_1 = 1$)

In this case, the free-space Green's function $G(z, z') = \frac{1}{i2k_0} e^{ik_0|z - z'|}$ should be used in the inhomogeneous Fredholm equations of first kind for $\Psi_0(z)$ and $\Psi_1(z)$ [4], namely,

$$\Psi_0(z) = \Psi_0^{(0)}(z) - k_0^2 \int_0^\infty dz' G(z,z') \left[n_2 |\Psi_1(z')|^2 + \frac{n_2^2}{4} |\Psi_1(z')|^4 \right] \Psi_1(z'); \quad z < 0 \quad (4)$$

and

$$\Psi_1(z) = \Psi_1^{(0)}(z) - k_0^2 \int_0^\infty dz' G(z,z') \left[n_2 |\Psi_1(z')|^2 + \frac{n_2^2}{4} |\Psi_1(z')|^4 \right] \Psi_1(z'); \quad z \geq 0 \quad (5)$$

where $\Psi_0^{(0)}(z)$ and $\Psi_1^{(0)}(z)$, which are also equal to the incident plane wave $e^{ik_0 z}$ for this case, are the unperturbed fields in regions 0 and 1, respectively. Since the contribution due to $-k_0^2 \left[n_2 |\Psi_1(z)|^2 + \frac{n_2^2}{4} |\Psi_1(z)|^4 \right] \Psi_1(z)$ to the scattered fields is very small, we can apply a perturbation method to expand the total fields of Eqs. (4) and (5) in terms of the unperturbed fields, namely,

$$\Psi_m(z) \approx \Psi_m^{(0)}(z) - k_0^2 \int_0^\infty dz' G(z,z') \Big[n_2 |\Psi_1^{(0)}(z') + \Psi_{1s}^{1BA}(z') + \Psi_{1s}^{2BA}(z') + ...|^2$$

$$+ \frac{n_2^2}{4} |\Psi_1^{(0)}(z') + \Psi_{1s}^{1BA}(z') + \Psi_{1s}^{2BA}(z') + ...|^4 \Big] \Big[\Psi_1^{(0)}(z') + \Psi_{1s}^{1BA}(z') + \Psi_{1s}^{2BA}(z') + ... \Big]$$

$$m = 0, 1 \qquad (6)$$

where $\Psi_{1s}^{nBA}(z)$ ($n = 1, 2, ...$) is the nth-order Born approximated scattered field in region 1. After lengthy calculation, we obtain the first-order and the second-order Born approximated scattered fields in region 0 and 1:

$$\Psi_{0s}^{1BA}(z) = - \frac{n_2}{4} e^{-ik_0 z}; \qquad\qquad z < 0, \quad (7a)$$

$$\Psi_{0s}^{2BA}(z) = \frac{3n_2^2}{16} e^{-ik_0 z}; \qquad\qquad z < 0, \quad (7b)$$

$$\Psi_{1s}^{1BA}(z) = \left(- \frac{n_2}{4} + i \frac{n_2}{2} k_0 z \right) e^{ik_0 z}; \qquad\qquad z \geq 0, \quad (8a)$$

and

$$\Psi_{1s}^{2BA}(z) = \left(\frac{3n_2^2}{16} - i \frac{3 n_2^2}{8} k_0 z - \frac{n_2^2}{8} k_0^2 z^2 \right) e^{ik_0 z}; \qquad z \geq 0. \quad (8b)$$

1.2. Exact Solutions of $\Psi_0(z)$ and $\Psi_1(z)$ for the 1-D Half-space Nonlinear Case with $n_0(z) = 1$ and $\varepsilon_1 = \varepsilon_0$ ($n_1 = 1$)

The closed-form solutions for $\Psi_0(z)$ and $\Psi_1(z)$ can be written as

$$\Psi_0(z) = e^{ik_0 z} + R_s e^{-ik_0 z}; \qquad\qquad z < 0 \quad (9)$$

and

$$\Psi_1(z) = T_s e^{ik_s z}; \qquad\qquad z \geq 0. \quad (10)$$

The real reflection and transmission coefficients, R_s and T_s, can be derived from the boundary conditions:

$$\Psi_0'(0) = \Psi_1(0) \tag{11}$$

and

$$\left.\frac{d\Psi_0(z)}{dz}\right|_{z=0} = \left.\frac{d\Psi_1(z)}{dz}\right|_{z=0}. \tag{12}$$

These boundary conditions can be applied for the acoustic case or the TE case in the electromagnetic wave theory. Since the wavenumber in the nonlinear medium is $k_s = k_0\left(1 + \frac{n_2}{2} T_s^2\right)$, the boundary conditions yield two equations for R_s and T_s, i.e.,

$$1 + R_s = T_s \tag{13a}$$

and

$$1 - R_s = \left(1 + \frac{n_2}{2} T_s^2\right) T_s \tag{13b}$$

from which we obtain

$$n_2 T_s^3 + 4 T_s - 4 = 0. \tag{14}$$

Eq. (14) has one real root given as

$$T_s = \left(\frac{2}{n_2} + \sqrt{\frac{64}{27n_2^3} + \frac{4}{n_2^2}}\right)^{1/3} - \frac{4}{3n_2\left(\frac{2}{n_2} + \sqrt{\frac{64}{27n_2^3} + \frac{4}{n_2^2}}\right)^{1/3}} \tag{15}$$

and two complex roots which are complex conjugate each other. The real root of Eq. (14) gives the correct approximation for the total fields when $n_2 \ll 1$, namely,

$$\Psi_0(z) \overset{n_2 \ll 1}{\approx} e^{ik_0z} + \left(-\frac{n_2}{4} + \frac{3n_2^2}{16} - \dots\right)e^{-ik_0z} \tag{16}$$

and

7

$$\Psi_1(z) \overset{n_2 \ll 1}{\approx} \left(1 - \frac{n_2}{4} + i\frac{n_2}{2}k_0 z + \frac{3n_2^2}{16} - i\frac{3n_2^2}{8}k_0 z - \frac{n_2^2}{8}k_0^2 z^2 - \dots \right) e^{ik_0 z}. \qquad (17)$$

Note that Eqs. (16) and (17) are exactly equal to the Born approximated fields derived from Eqs. (4) and (5).

1.3. The Born Method for the 1-D Half-space Nonlinear Case with $n_0(z) = 1$ and $\varepsilon_1 > \varepsilon_0$

In this case, the Green's functions, $G_{00}(z, z')$, $G_{10}(z, z')$, $G_{01}(z, z')$, and $G_{11}(z, z')$ which are governed by the equations

$$\frac{d^2 G_{pq}(z, z')}{dz^2} + k_p^2 G_{pq}(z, z') = \delta_{pq}\delta(z - z'); \qquad (p, q = 0, 1) \quad (18)$$

are used in the inhomogeneous Fredholm equations of first kind for $\Psi_0(z)$ and $\Psi_1(z)$. Note that δ_{pq} is the Kronecker delta and $\delta(z - z')$ is the delta function. Physically, $G_{pq}(z, z')$ describes how the field, generated by a point source at z' (in region q), behaves at the observation location z (in region p). From the boundary conditions at $z = 0$:

$$G_{pp}(0, z') = G_{qp}(0, z') \qquad (19)$$

and

$$\left.\frac{dG_{pp}(z, z')}{dz}\right|_{z=0} = \left.\frac{dG_{qp}(z, z')}{dz}\right|_{z=0} \qquad (20)$$

where p, q = 0, 1 and $q \neq p$, we obtain

$$G_{00}(z, z') = \frac{1}{i2k_0}\left[e^{ik_0|z - z'|} + R(k_1)e^{-ik_0(z + z')} \right]; \qquad z \ \& \ z' < 0, \quad (21)$$

8

$$G_{10}(z, z') = \frac{1}{i2k_0} \cdot T(k_1) e^{ik_1 z} e^{-ik_0 z'}; \qquad\qquad z' < 0 \leq z, \quad (22)$$

$$G_{11}(z, z') = \frac{1}{i2k_1} \left[e^{ik_1 |z - z'|} - R(k_1) e^{ik_1(z + z')} \right]; \qquad z \,\&\, z' \geq 0, \quad (23)$$

and

$$G_{01}(z, z') = \frac{1}{i2k_0} T(k_1) e^{-ik_0 z} e^{ik_1 z'}; \qquad\qquad z < 0 \leq z'. \quad (24)$$

Note that the coefficients

$$R(k_1) = \frac{k_0 - k_1}{k_0 + k_1} \tag{25}$$

and

$$T(k_1) = \frac{2k_0}{k_0 + k_1}. \tag{26}$$

are the same as the reflection and the transmission coefficents in the three-dimensional case for a TE wave normally incident on a dielectric half-space with permittivity ε_1. Owing to the symmetry of the scattering geometry in the dielectric half-space case, the Green's functions satisfy the symmetry properties [5], namely,

$$G_{pq}(z, z') = G_{qp}^{T}(z', z); \qquad (p, q = 0, 1). \quad (27)$$

Therefore, the total field $\Psi_p(z)$ in region p (0 or 1) can be expressed as

$$\Psi_p(z) = \Psi_p^{(0)}(z) - k_1^2 \int_0^\infty dz' G_{p1}(z, z') \left[\frac{n_2}{n_1} |\Psi_1(z')|^2 + \frac{n_2^2}{4n_1^2} |\Psi_1(z')|^4 \right] \Psi_1(z') \tag{28}$$

where in this case, the unperturbed fields, $\Psi_0^{(0)}(z)$ and $\Psi_1^{(0)}(z)$, are equal to $e^{ik_0 z}$ and $T(k_1) e^{ik_1 z}$, respectively. After applying the perturbation method to expand

9

Eq. (28) into the Born series simliar to Eq. (6) and using Eqs. (23) and (24), we obtain the first- and the second-order Born approximated scattered fields

$$\Psi_{0s}^{1BA}(z) = -\frac{n_2}{4} T^4(k_1) e^{-ik_0 z}; \qquad\qquad z < 0, \quad (29a)$$

$$\Psi_{0s}^{2BA}(z) = \frac{3n_2^2}{16} T^7(k_1) e^{-ik_0 z}; \qquad\qquad z < 0, \quad (29b)$$

$$\Psi_{1s}^{1BA}(z) = \left[-\frac{n_2}{4} T^4(k_1) + i \frac{n_2}{2n_1} T^3(k_1)k_1 z \right] e^{ik_1 z}; \qquad z \geq 0, \quad (30a)$$

and

$$\Psi_{1s}^{2BA}(z) = \left[\frac{3n_2^2}{16} T^7(k_1) - i \frac{3n_2^2}{8n_1} T^6(k_1)k_1 z - \frac{n_2^2}{8n_1^2} T^5(k_1)k_1^2 z^2 \right] e^{ik_1 z}; \quad z \geq 0. \quad (30b)$$

1.4. Exact Solutions of $\Psi_0(z)$ and $\Psi_1(z)$ for the 1-D Half-space Nonlinear Case with $n_0(z) = 1$ and $\epsilon_1 > \epsilon_0$

Similar to Eqs. (9) and (10), $\Psi_0(z)$ and $\Psi_1(z)$ can be written as

$$\Psi_0(z) = e^{ik_0 z} + R_d e^{-ik_0 z}; \qquad\qquad z < 0 \qquad (31)$$

and

$$\Psi_1(z) = T_d e^{ik_d z}; \qquad\qquad z \geq 0 \qquad (32)$$

where $k_d = k_1 \left(1 + \frac{n_2}{2n_1} T_d^2 \right)$. Using the same boundary conditions as in Eqs. (11) and (12), we can derive two relations for R_d and T_d from which we obtain

$$n_2 T_d^3 + \frac{4}{T(k_1)} T_d - 4 = 0. \qquad\qquad (33)$$

Eq. (33) has also one real root given as

10

$$T_d = \left(\frac{2}{n_2} + \sqrt{\frac{64}{27 n_2^3 \, T^3(k_1)} + \frac{4}{n_2^2}}\right)^{1/3} - \frac{4}{3 n_2 \left(\frac{2}{n_2} + \sqrt{\frac{64}{27 n_2^3 \, T^3(k_1)} + \frac{4}{n_2^2}}\right)^{1/3}} \quad (34)$$

and two complex roots. Thus, with Eq. (34) and the condition that $n_2 \ll 1$, the total fields can be approximated as

$$\Psi_0(z) \overset{n_2 \ll 1}{\approx} e^{ik_0 z} + \left(-\frac{n_2}{4} T^4(k_1) + \frac{3 n_2^2}{16} T^7(k_1) - \dots\right) e^{-ik_0 z} \quad (35)$$

and

$$\Psi_1(z) \overset{n_2 \ll 1}{\approx} \left[1 - \frac{n_2}{4} T^4(k_1) + i \frac{n_2}{2 n_1} T^3(k_1) k_1 z + \frac{3 n_2^2}{16} T^7(k_1) - i \frac{3 n_2^2}{8 n_1} T^6(k_1) k_1 z\right.$$

$$\left. - \frac{n_2^2}{8 n_1^2} T^5(k_1) k_1^2 z^2 - \dots\right] e^{ik_1 z}. \quad (36)$$

Eqs. (35) and (36) are exactly equal to the Born approximated fields in Eqs. (29a) to (30b).

2. Image Reconstructions for RADC Bistatic Scattering Measurements

In a previous report (October 1, 1990 to April 8, 1991), we applied the far-field filtered backpropagation algorithm to reconstruct, from the far-field scattered data taken at the RADC bistatic scattering experiments, the images of two empty annular cardboard cylinders with 8.5 cm and 15 cm in diameter and 0.4 cm in thickness. These reconstructions are accomplished by backpropagating 36 sets of 10 GHz scattered field data $\Psi_s(\bar{\rho}_s, k\beta_o)$ into the scatterer domain. Each set of data, containing 181 data points, corresponds to one viewing direction; the viewing angle ranges from $0°$ to $350°$ with $10°$ increments. Each data point within each set of data corresponds to one scattering angle; the scattering angle ranges from $0°$ to $180°$ with $1°$ increment. Before using the far-field backpropagation algorithm resulted from Eq. (23) of the previous report, the scattered data is interpolated into the cartesian grid on the k-domain in order to apply the fast Fourier transform. The interpolation module (the IMSL subroutine "IQHSCV") involves a smoothing process. Also the summation over all viewing angles (using Eq. (23) of the April 1991 report) combines both the along- and the across-viewing-direction structures of $V(\bar{\rho})\Psi(\bar{\rho})$ for all views (where $V(\bar{\rho})$ is the scattering function and $\Psi(\bar{\rho})$ is the total field in the scatterer). Therefore, both the along- and the across-viewing-direction structures of $V(\bar{\rho})\Psi(\bar{\rho}, k_0\beta_o)$ for each view with the viewing direction β_o have been artificially symmetrized. Although the far-field backpropagation algorithm provides a way of fast reconstruction, the brute-force method is necessary to integrate Eq. (20) of the April 1991 report in order to reconstruct the true along- and the across-viewing-direction structures of $V(\bar{\rho})\Psi(\bar{\rho}, k_0\beta_o)$.

Suppose that the scattered field data, $\Psi_s(\bar{\rho}_s, k_0\beta_o)$, were measured in the far-field at positions $\bar{\rho}_s = \rho_s (\hat{x} \cos\varphi_s + \hat{y} \sin\varphi_s)$ after the scatterer had been

illuminated by a time-harmonic plane wave of wavenumber k_0 propagating in the direction $\hat{\beta}_o = \hat{x} \cos\varphi_o + \hat{y} \sin\varphi_o$. In 2D diffraction tomography, we have shown [6] that the scattered field $\Psi_s(\bar{\rho}_s, k_0\hat{\beta}_o)$ is written as,

$$\Psi_s(\bar{\rho}_s, k_0\hat{\beta}_o) = \frac{ik_0^2}{4} \int_\Omega d^2\bar{\rho}\,' \, H_0^{(1)}(k_0|\bar{\rho}_s - \bar{\rho}\,'|)V(\bar{\rho}\,')\Psi(\bar{\rho}\,', k_0\hat{\beta}_o) \tag{37}$$

where $H_0^{(1)}(k_0|\bar{\rho}_s - \bar{\rho}\,'|)$ is the zeroth order of the Hankel function of first kind and the integration is over the cross section Ω of the scatterer. Under the far-field approximation, we have

$$H_0^{(1)}(k_0|\bar{\rho}_s - \bar{\rho}\,'|) \approx \frac{4}{i}\sqrt{\frac{1}{8\pi k_0\rho_s}} e^{i(k_0\rho_s + \pi/4)}\, e^{-ik_0\hat{\beta}_s\cdot\bar{\rho}\,'} \tag{38}$$

and, thus

$$\Psi_s(\bar{\rho}_s, k_0\hat{\beta}_o) \approx \sqrt{\frac{k_0^3}{8\pi\rho_s}} e^{i(k_0\rho_s + \pi/4)} \int_\Omega d^2\bar{\rho}\,' e^{-ik_0\hat{\beta}_s\cdot\bar{\rho}\,'} V(\bar{\rho}\,')\Psi(\bar{\rho}\,', k_0\hat{\beta}_o). \tag{39}$$

By defining a function

$$f(\bar{\rho}, k_0\hat{\beta}_o) = V(\bar{\rho})\Psi(\bar{\rho}, k_0\hat{\beta}_o)\, e^{-ik_0\hat{\beta}_o\cdot\bar{\rho}} \tag{40}$$

then, Eq. (39) can be rewritten as

$$F_{\varphi_o}(\bar{K}) = \frac{1}{4\pi^2} \int_\Omega d^2\bar{\rho}\,' e^{-ik_0\hat{\beta}_s\cdot\bar{\rho}\,'} \, f(\bar{\rho}\,', k_0\hat{\beta}_o)\, e^{ik_0\hat{\beta}_o\cdot\bar{\rho}\,'} \tag{41}$$

where

$$F_{\varphi_o}(\bar{K}) \equiv \sqrt{\frac{\rho_s}{2\pi^3 k_0^3}} e^{-i(k_0\rho_s + \pi/4)} \, \Psi_s(\bar{\rho}_s, k_0\hat{\beta}_o) \tag{42a}$$

and

$$\bar{K} = \hat{x}k_0\left(\cos\varphi_s - \cos\varphi_o\right) + \hat{y}k_0\left(\sin\varphi_s - \sin\varphi_o\right). \tag{42b}$$

After taking the inverse Fourier transform of Eq. (41), we obtain

$$f(\bar{\rho}, k_0\hat{\beta}_o) = \int\limits_{-\infty}^{\infty}dK_x \int\limits_{-\infty}^{\infty}dK_y e^{i(K_x x + K_y y)} F_{\varphi_o}(K_x, K_y). \tag{43}$$

In fact, the limits of integration in Eq. (43) can only be from $-2k_0$ to $2k_0$ because the measured data $F_{\varphi_o}(K_x, K_y)$ are confined within a disc centered at the origin and having a radius $2k_0$ on the k-domain. If we transform the integration $dK_x dK_y$ to $d\varphi_o d\varphi_s$ by using the relations:

$$K_x = k_0\left(\cos\varphi_s - \cos\varphi_o\right) \tag{44a}$$

and

$$K_y = k_0\left(\sin\varphi_s - \sin\varphi_o\right), \tag{44b}$$

Eq. (43) becomes

$$V(\bar{\rho})\Psi(\bar{\rho}) = \frac{k_0^2}{2} \int\limits_{0}^{2\pi}d\varphi_o \int\limits_{0}^{2\pi}d\varphi_s\, e^{ik_0(\hat{\rho}_s - \hat{\rho}_o)\cdot\bar{\rho}} \sqrt{1 - (\hat{\rho}_s - \hat{\rho}_o)^2}\, F_{\varphi_o}(k_0(\hat{\rho}_s - \hat{\rho}_o)). \tag{45}$$

which is the same as Eq. (20) of the previous report that is used to formulate the far-field filtered backpropagation algorithm. Note that the dependence of the viewing angle in $\Psi(\bar{\rho}, k_0\hat{\beta}_o)$ is averaged out in Eq. (45). However, if only one viewing angle is considered in Eq. (45), we can reconstruct the along- and across-viewing-direction structures of $V(\bar{\rho})\Psi(\bar{\rho}, k_0\hat{\beta}_o)$.

14

In Figures 2 to 7, the 2-D grey-level images are the modulus plots reconstructed, from two sets of simulated and two sets of measured scattered field data, over a spatial area 64×64 cm^2 in the object domain while the 1-D linear plots are real parts of the corresponding images either along or across the viewing direction. For comparison, the actual size of each cylinder is indicated by the tip of the arrowhead on each 2-D grey-level plot. Figures 2a and 3a are the reconstructions, from simulated scattered field data, of cross sections for solid cylinders both having V = 0.03 and with 4.25 cm and 15 cm in radius, respectively. Figures 2b and 3b (2c and 3c) are the along-viewing-direction (the across-viewing-direction) plots of the real parts for the objects corresponding to Figure 2a and 3a along the line y = 0 (x = 0). Figures 4a and 5 are the reconstructions, respectively from measured scattered field data for incident angle (or viewing angle) at 0° and 240°, of cross section for the annular cardboard cylinder having a radius 4.25 cm, thickness 0.4 cm, and filled with styrofoam of V = 0.03. Figure 4b and 4c are the along- and the across-viewing-direction plots of the real parts for the object corresponding to Figure 4a along the lines y = 0 and x = 0, respectively. Figures 6a and 7a are the reconstructions, respectively from measured scattered field data for incident angle at 0° and 90°, of cross section for the empty annular cardboard cylinder having a radius 15 cm and thickness 0.4 cm. Figures 6b and 7b (6c and 7c) are the along-viewing-direction (the across-viewing-direction) plots of the real parts for the objects corresponding to Figure 6a and 7a along the line y = 0 (x = 0). Note that after the filtering algorithm has been applied to remove noise from experimental data, we are able to obtain consistent reconstructions for two different viewing directions; comparing Figures 6b and 6c with Figures 7b and 7c.

viewing direction →
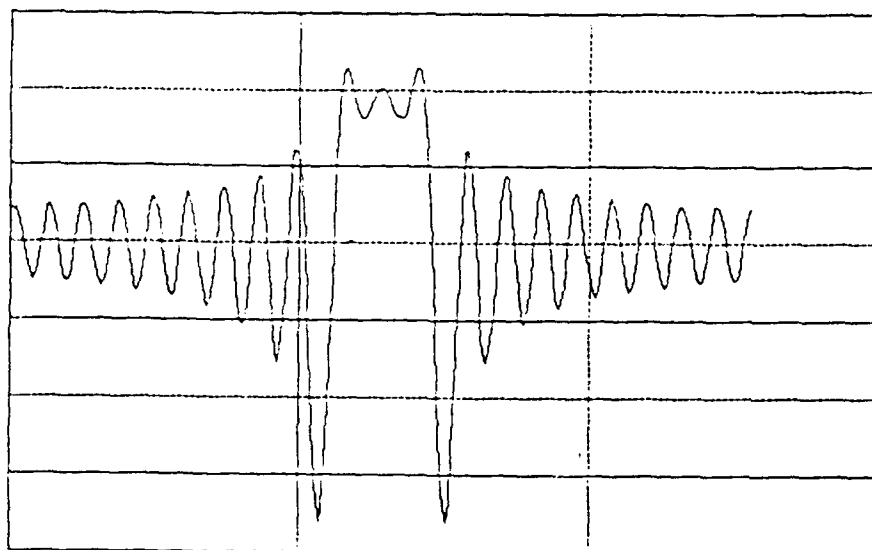
Figure 2a.

Figure 2b.
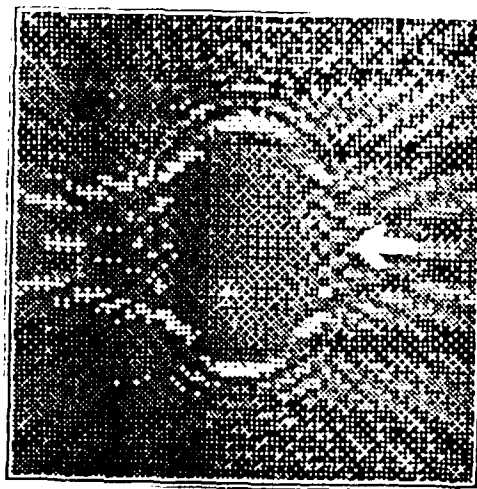

Figure 2c.

viewing direction →

Figure 3a.
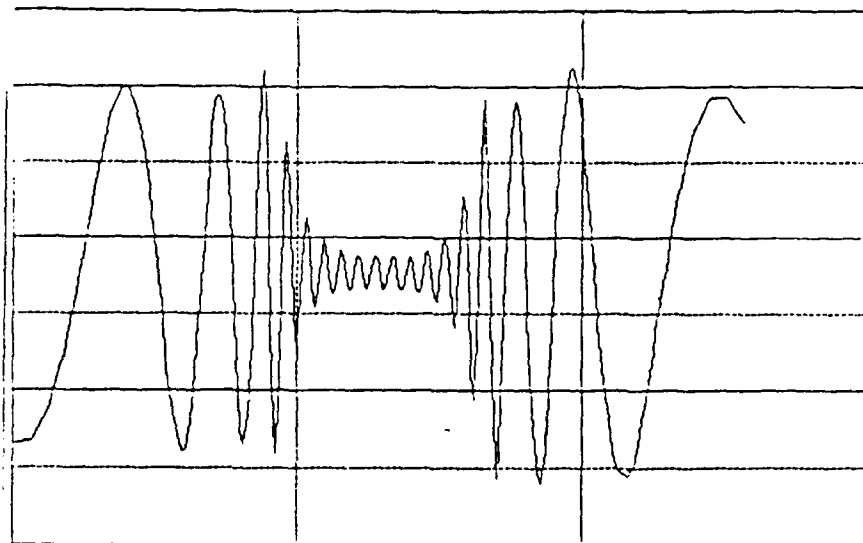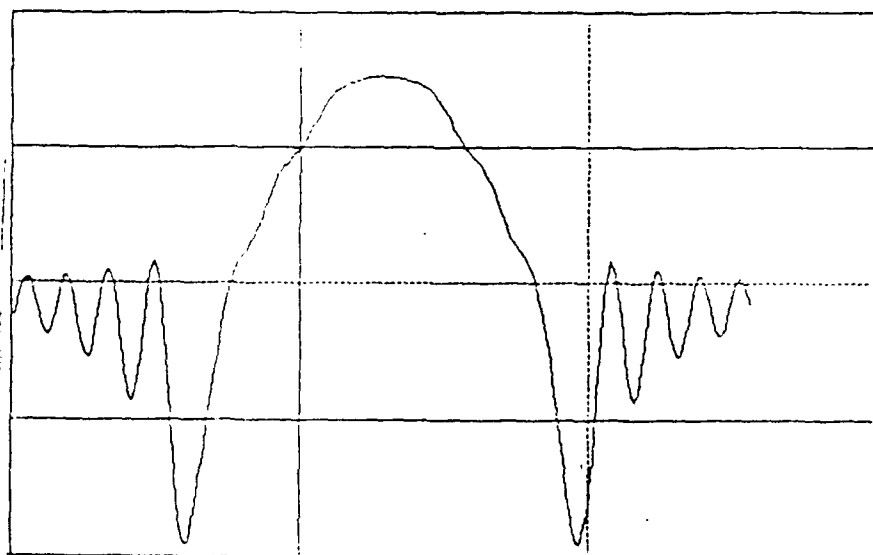

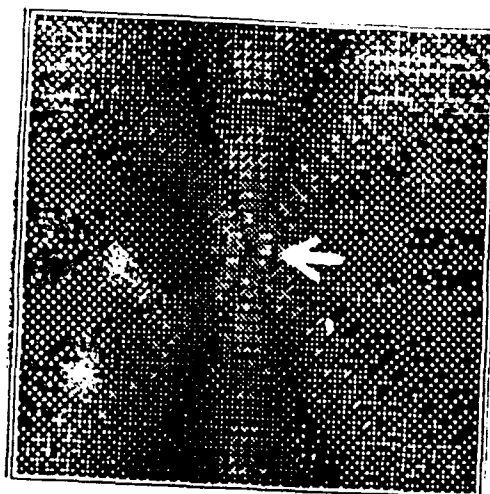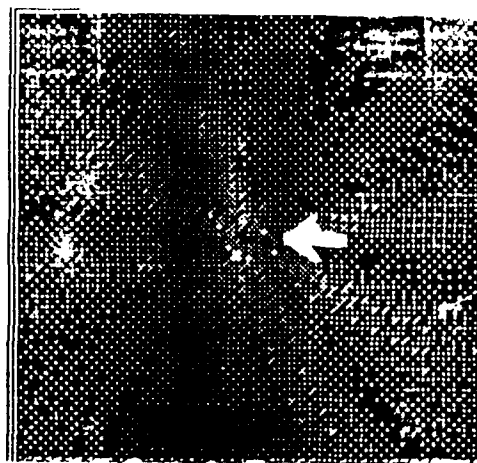Figure 3b.

Figure 3c.

17

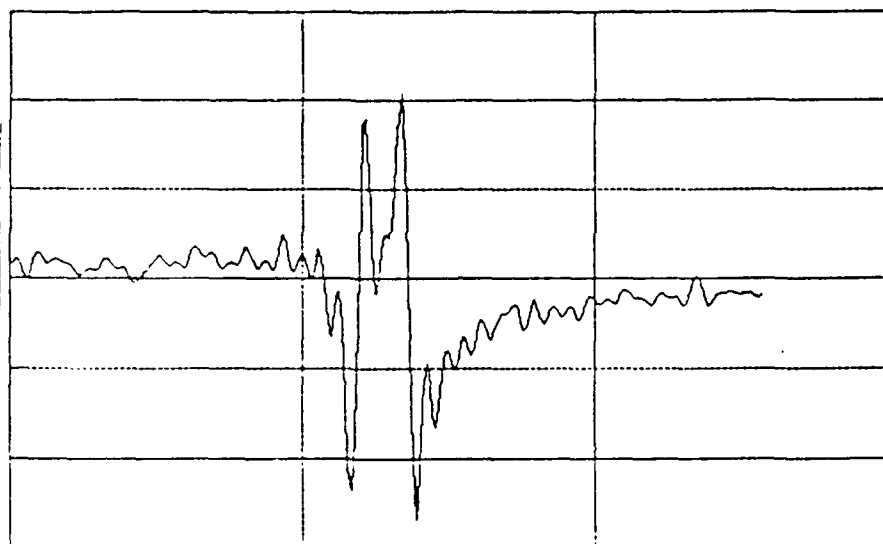viewing direction →

Figure 4a.
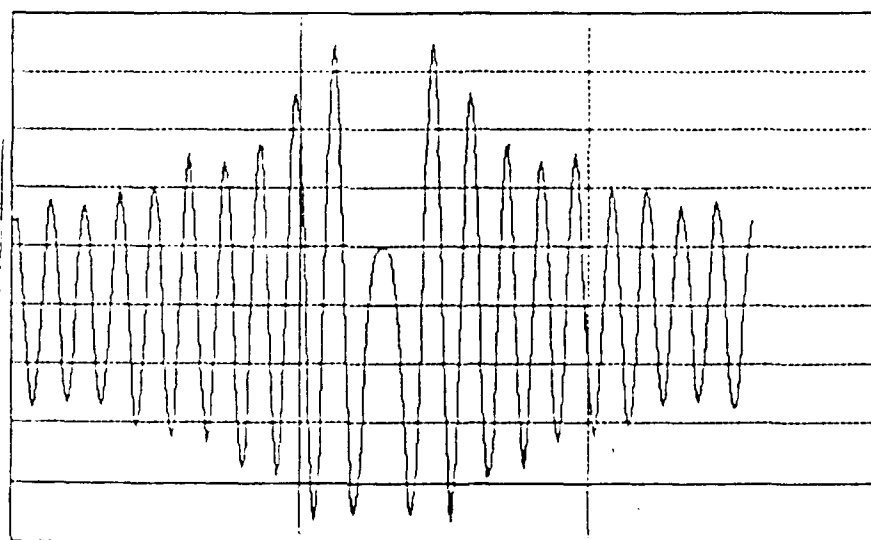

Viewing direction

Figure 5.
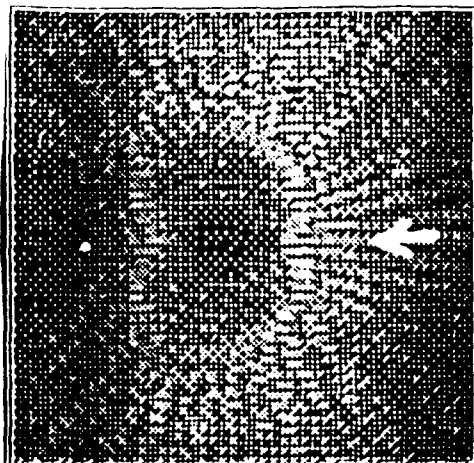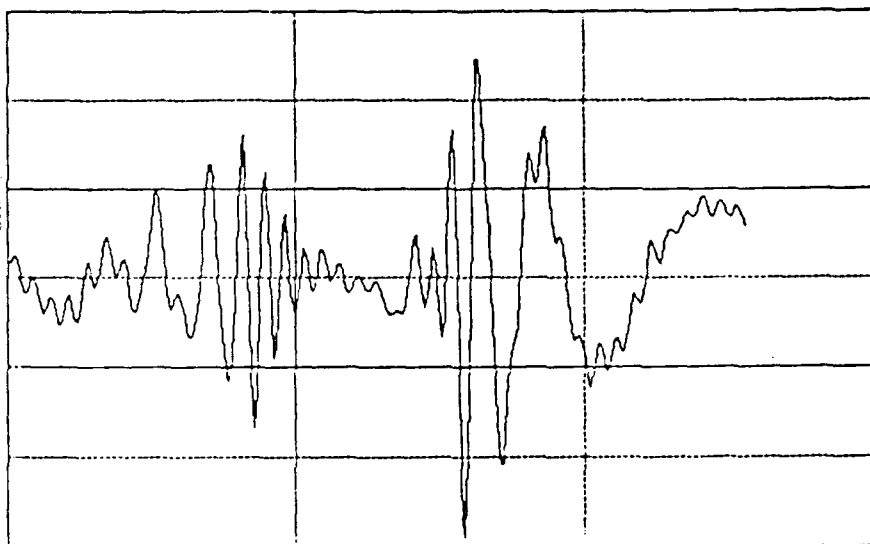

Figure 4b.

Figure 4c.

viewing direction →

Figure 6a.
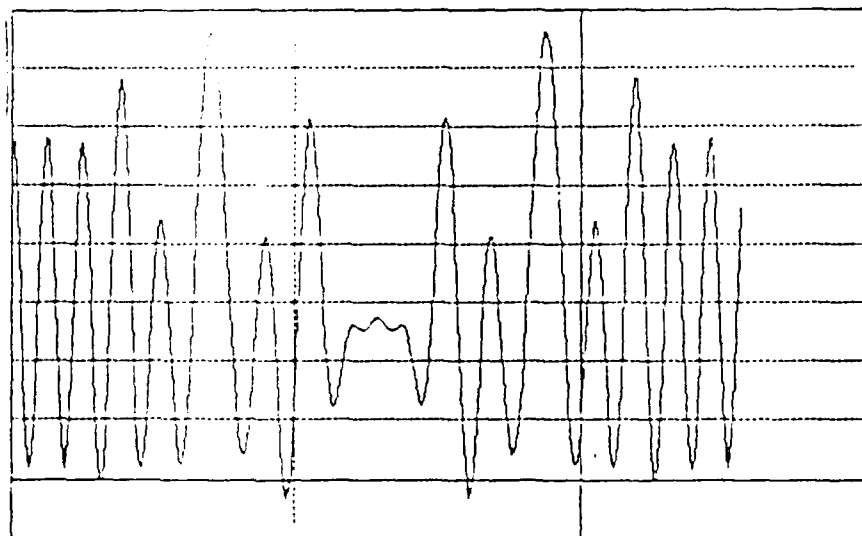

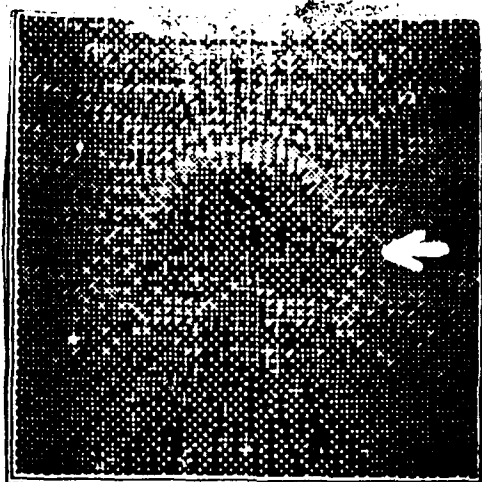Figure 6b.

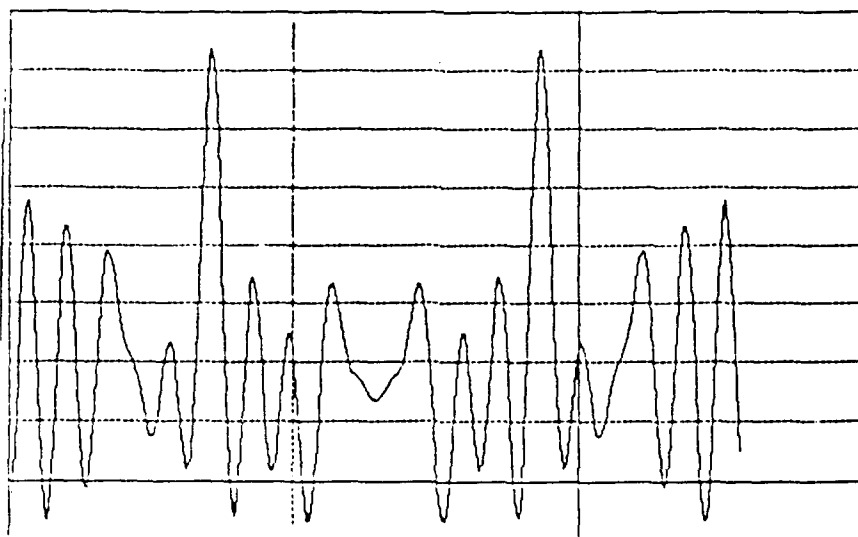
Figure 6c.

viewing direction →

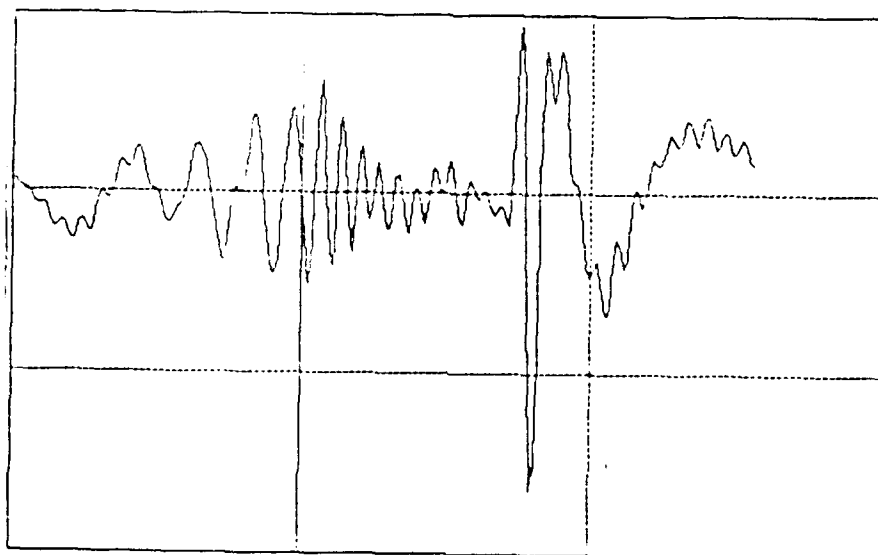Figure 7a.

Figure 7b.

Figure 7c.

20

References

1. P. W. Smith, P. J. Maloney, and A. Ashkin, "Use of a liquid suspension of dielectric spheres as an artificial Kerr medium," Opt. Lett., 7, 347-349, (1982).

2. S. A. Akhmanov, R. V. Khokhlov, and A. P. Sukhorukov, "Self-focusing, self-defocusing and self-modulation of laser beams," in Laser Handbook, Vol. 2, edited by F. T. Arecchi and E. O. Schulz-Dubois, North-Holland Publishing Co., Amsterdam, 1152-1228, (1972).

3. A. Ashkin, J. M. Dziedzic, and P. W. Smith, "Continuous-wave self-focusing and self-trapping of light in artificial Kerr media," Opt. Lett., 7, 276-278, (1982).

4. F. C. Lin and M. A. Fiddy, "On the issue of the Born-Rytov controversy: I. Comparing analytical and approximate expressions for the one-dimensional deterministic case," accepted for publication in J. Opt. Soc. Am., A, (1992).

5. C. T. Tai, Dyadic Green's Functions in Electromagnetic Theory, (Intex Educational Publishers, Scranton, PA, 1971).

6. F. C. Lin and M. A. Fiddy, "Image estimation from scattered field data," Int. J. Imaging Systems and Technology, 2, 76-95, 1990.

Summary of work directions in the next period

The following areas will be pursued in the next few months:

i) Homomorphic filtering techniques applied to the inverse scattering problem, for simulated and real data.

ii) Inversion of data for the recovery of nonlinear permittivity profiles, with the expectation that we can design permittivity structures in nonlinear media such as photorefractives.